Astron. Astrophys. 231, 473–480 (1990)

ASTRONOMY AND ASTROPHYSICS

Molecules and masers near compact H II regions

J.R. Forster[1], J.L. Caswell[2], S.K. Okumura[3], T. Hasegawa[4], and M. Ishiguro[3]

[1] Australia Telescope National Facility, CSIRO-Paul Wild Observatory, P.O. Box 94, Narrabri NSW 2390, Australia
[2] Australia Telescope National Facility, CSIRO-Division of Radiophysics, P.O. Box 76, Epping NSW 2121, Australia
[3] Nobeyama Radio Observatory, National Astronomical Observatory, Nobeyama, Minamisaku, Nagano 348-13, Japan
[4] Institute of Astronomy, University of Tokyo, Mitaka, Tokyo 181, Japan

Received March 28, accepted July 19, 1989

Abstract. Nine compact H II regions with OH/H_2O masers were observed in hydrogen recombination line and molecular line emission at 40, 90 and 110 GHz with the Nobeyama 45m telescope. The recombination line emission occurs at a velocity offset with respect to the molecular lines by typically ± 6 km s^{-1}. High-velocity H_2O masers tend to occur at velocities shifted in the opposite sense from the recombination lines. We suggest that the molecular gas is relatively stationary in these star-forming regions, and the ionized hydrogen is expanding asymmetrically into regions of lower density. High-velocity H_2O masers move in the direction of increasing density, probably excited by collisions with ambient molecular material.

Key words: star formation – masers – molecules – H II regions – radio recombination lines

1. Introduction

Compact H II regions represent a late stage of massive star formation in which a substantial volume of gas surrounding a young star becomes ionized. The development of a detectable H II region may coincide with the end of the accretion phase. While the star is accreting, ultraviolet photons are used up in maintaining the ionization balance for a continuing supply of gas. When the inflow of material stops, the ionization front moves out as the luminosity of the star increases. At the same time the H II region expands due to its high internal pressure. The expanding H II region, along with radiation pressure and mass outflow from the star, eventually disperses the surrounding gas and dust, and the star emerges as a visible object.

The early evolutionary stage of massive star formation cannot be observed optically due to heavy obscuration, and arcsecond or better resolution is needed at radio and infrared wavelengths to resolve most compact H II regions. The radio continuum observations with sufficient resolution made in recent years show a variety of structures, including complete or partial shells, cometary shapes and irregular morphologies (Wood and Churchwell, 1989). One implication of these observations is a more complex interaction between the emerging young star and its surroundings than is suggested by simple spherical expansion. The presence of bipolar outflows in both molecular and ionized gas, high-velocity masers, and shock-excited molecular hydrogen provide further evidence of a complex and energetic interaction.

In order to study the kinematics of young star-forming regions the systemic velocity of the region is of fundamental importance. While maser transitions of OH and H_2O are easy to observe, their generally complex spectra and wide velocity spread complicates their use for this purpose. Strong thermal lines such as CO are sometimes used, but the molecules producing these lines are so plentiful that confusion and optical depth effects can be a problem. High-excitation lines such as NH_3 are more useful because they selectively probe high-density gas. When an H II region is present, the hydrogen recombination line velocity is generally held as the best estimate of the systemic velocity of the star-forming region. However, optical depth effects and internal motions in the ionized gas can influence the measurements at low frequencies.

We have selected nine compact H II regions with OH and H_2O maser emission, and three OH/H_2O maser associations without detectable H II regions, to further investigate the kinematics of young star-forming regions. These objects have been previously mapped at high resolution in the radio continuum and the maser lines. In this study, two recombination lines and several molecular lines were observed with the Nobeyama 45m radiotelescope. The relationship between the H II region, the surrounding molecular gas, and the masers is discussed in light of the new results.

2. Observations

The observations were carried out in two 12 hour sessions on 20 and 21 May, 1987 using the 45m radiotelescope of the Nobeyama Radio Observatory[1]. The observed sources are listed in Table 1 with galactic coordinates used as source names in most cases. We refer to these sources by their galactic coordinates only, rather than using G, OH or H_2O prefixes, since we generally refer to the complex as a whole. The spectral lines observed are given in

Send offprint requests to: J.R. Forster

[1] The Nobeyama Radio Observatory (NRO) is a branch of the National Astronomical Observatory, Ministry of Education, Science and Culture of Japan, and is a facility open for general use by researchers in the fields of astronomy, astrophysics and astrochemistry.

Table 1. Sources observed

Source	RA (1950)	Dec (1950)	H II (Jy)	D (kpc)	Ref.
W3 (OH)	$02^h23^m16^s5$	61°38′57″	2.1	3.0	6–11
351.41+0.64	17 17 32.3	−35 44 04	2.4	1.9	1, 3, 12
351.58−0.35	17 22 03.2	−36 10 06	1.0	9.9	1
351.78−0.54	17 23 20.3	−36 06 44	<0.2	2.2	1
0.54−0.85	17 47 03.8	−28 53 40	<0.2	2.0	1
5.88−0.39	17 57 26.7	−24 03 57	6.3	2.6	1, 18
8.68−0.37	18 03 18.8	−21 37 53	0.9	5.8	1
10.62−0.38	18 07 30.6	−19 56 30	2.0	6.0	1, 2, 4, 5, 18
34.26+0.15	18 50 46.1	01 11 13	5.0	4.2	1, 2, 3, 14
45.07+0.13	19 11 00.4	10 45 43	0.8	10.0	1, 2, 4, 5
45.47+0.13	19 11 46.0	11 07 03	<0.2	9.3	1
NGC 7538	23 11 36.6	61 11 50	0.4	3.3	15, 16, 17

References: (1) Forster and Caswell, 1988; (2) Garay et al., 1985; (3) Gaume and Mutel, 1987; (4) Ho et al., 1983; (5) Turner and Matthews, 1984; (6) Reid et al., 1980; (7) Norris and Booth, 1981; (8) Dreher and Welch, 1981; (9) Welch and Marr, 1987; (10) Berulis and Ershov, 1983; (11) Wilson et al., 1987; (12) Rodriguez et al., 1982; (13) Ho and Haschick, 1981; (14) Benson and Johnston, 1984; (15) Rots et al., 1981; (16) Campbell, 1984; (17) Forster et al., 1978; (18) Wood and Churchwell, 1988

Table 2. Spectral lines observed

Species	Transition	Frequency (MHz)	E (K)	A (s^{-1})
Recombination lines				
Hα	54−53	42951.97	56	1.16 (+1)
Hα	42−41	92034.45	94	6.23 (+7)
Detected molecules				
SiO	1−0 v=0	43423.85	2	3.06 (−6)
HNCO	2 (0, 2)–1 (0, 1)	43963.00		
CH_3OH	7 (0)–6 (1) A^+	44069.49	65	3.94 (−5)
HCN	1−0	88631.85	4	2.43 (−5)
HCO^+	1−0	89188.52	4	3.02 (−5)
CH_3CN	5 (2)–4 (2)	91980.09	42	5.31 (−5)
^{13}CO	1−0	110201.35	5	6.40 (−8)
Not detected				
HC_5N	16−15	42602.15	17	8.18 (−6)
SiO	1−0 v=2	42820.59	3522	3.00 (−6)
SiO	1−0 v=1	43122.08	1770	3.02 (−6)
CH_3OH	15 (3)–14 (4) A^+	88594.96		
CH_3CN	6 (2)–5 (2)	110349.66	133	6.16 (−5)
CH_3CN	6 (1)–5 (1)	110381.40	26	1.08 (−4)

Notes: The molecular frequencies and quantum assignments are taken from Lovas 1986; the recombination-line frequencies are from Lilley and Palmer 1968. The energy E of the upper state is expressed in K, and the (base 10) exponent of the Einstein A coefficient is given in parenthesis

Table 2. The beamsize at 40, 90 and 110 GHz was approximately 40″, 20″ and 15″ respectively.

Two receiver configurations were used: (A) simultaneous observations with the 40 and 80 GHz receivers covering 42.6–44.2 GHz and 91.9–92.4 GHz; and (B) simultaneous observations with the 80 and 100 GHz receivers covering 88.3–89.3 GHz and 110.0–110.5 GHz. The observations were made in position-switched mode, with the reference position offset from the source position by about 20′. Eight wideband (each 250 MHz bandwidth) and eight narrowband (40 MHz

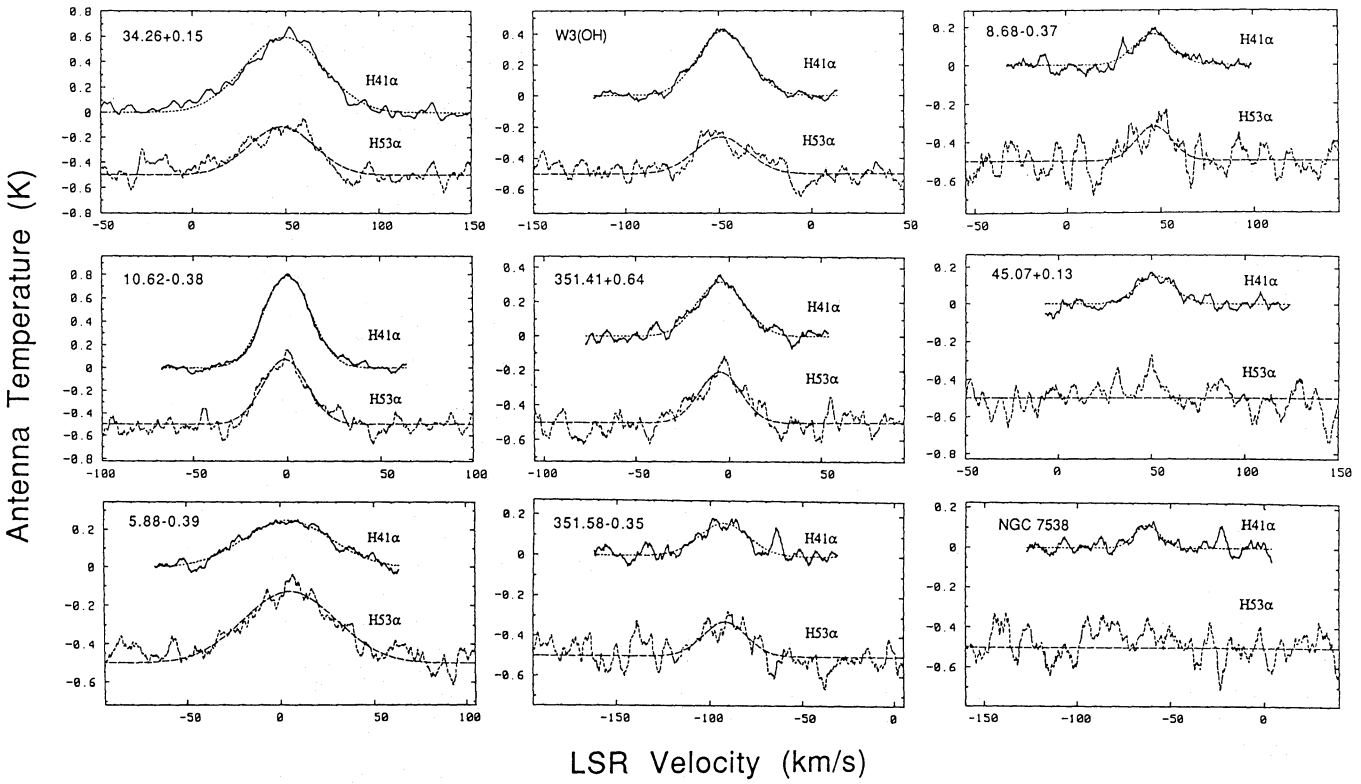

Fig. 1. H41α and H53α recombination line spectra for the nine sources with H II regions. The H53α spectra are shifted vertically by −0.5 K, and all spectra are smoothed to a resolution of 5 km s^{-1}. The sources are ordered with H41α total received power decreasing from top to bottom, left to right

bandwidth) 2000-channel acousto-optical spectrometers were employed. Configuration A was used for recombination line and weak molecular line measurements, and long (~1 h) integrations were made at the source position. In configuration B, which covered the strong transitions of ^{13}CO, HCO^+ and HCN, short integrations (~1 min) were made at the source position and at 30″ offsets in RA and Dec. For four sources observations were also made with offsets of 60″. The offset position data was acquired in order to determine the position and extent of molecular line emission.

3. Results

3.1. Recombination lines

H41α and H53α recombination line spectra toward nine H II regions are shown in Fig. 1. The spectra are arranged in order of decreasing H41α total received power ($\int T_a dv$), and they have been smoothed to a velocity resolution of 5 km s^{-1}. The H53α lines are of lower quality and usually lower amplitude than the H41α lines; the H53α line was not detected in two sources. Gaussian profiles have been fitted to each spectrum, and these are shown dashed in Fig. 1. The amplitude, velocity and width of the fitted profiles, along with their formal errors (shown subscripted), are listed in Table 3. The line shapes are essentially Gaussian, but slight departures from a Gaussian profile are present in some cases. This is particularly evident for 34.26 ± 0.15, and accounts for the high formal errors in the fit. Typical rms errors in velocity are ~0.8 km s^{-1} for H41α and ~1.2 km s^{-1} for H53α.

3.2 Molecular lines

Gaussian fit parameters for the detected molecules are given in Table 3. The sources are arranged in order of decreasing H41α total power as in Fig. 1, and the spectral lines are grouped with recombination lines at the left, weak, generally high-excitation molecules in the centre, and the strong lines observed in configuration B at the right. The lines were seen in emission, with the possible exception of HNCO which may be in absorption in a few cases. However, the absorption is at a low level of significance (~2σ) and is not included in Table 3.

The weakest of the detected lines is HNCO, with an average antenna temperature of 0.3 K. HNCO was clearly detected in three of the 12 sources observed. The ground state SiO line ($J=1-0$, $v=0$) was detected in seven sources at an average amplitude of 0.5 K. This line generally has a broader halfwidth than the other molecules. The vibrationally excited SiO lines ($v=1$ and $v=2$) were not detected. A group of five closely spaced CH_3CN lines near 92 GHz was detected in nine sources. The 5(2)–4(2) $F=6-5$ transition was chosen for Gaussian analysis because it has the smallest frequency spread due to hyperfine structure. Neither of the $J=6-5$ CH_3CN lines near 110 GHz were detected. An unexpected line near 92 GHz was detected toward 10.62−0.38; it is tentatively identified as $^{13}CH_3CH_2CN$.

The 7(0)–6(1) A^+ methanol (CH_3OH) line near 44 GHz was detected in all except two sources. These lines are strong (antenna temperatures ~1 to 15 K), and the spectra consist of narrow, multiple spikes similar to OH and H_2O masers. The large variation in intensity from source to source is also suggestive of

Table 3. Gaussian fit results

	H41α	H53α	SiO	CH_3CN	HNCO	CH_3OH	^{13}CO	HCO^+	HCN
34.26+0.15									
Amplitude (K)	$0.6_{0.2}$	$0.4_{0.1}$	$0.5_{0.1}$	$0.8_{0.1}$	<0.1	$2.3_{0.1}$	$12.0_{0.3}$	$6.9_{0.2}$	$3.7_{0.4}$
Velocity (km s^{-1})	$48.8_{1.4}$	$47.1_{0.9}$	$58.0_{0.3}$	$59.1_{0.1}$		$57.1_{0.1}$	$57.0_{0.1}$	$56.7_{0.1}$	$57.0_{0.2}$
FWHM (km s^{-1})	$50.1_{3.3}$	$42.4_{2.2}$	$7.2_{0.6}$	$6.8_{0.1}$		$4.7_{0.2}$	$3.9_{0.1}$	$2.8_{0.1}$	$2.4_{0.4}$
10.62−0.38									
Amplitude (K)	$0.8_{0.1}$	$0.6_{0.1}$	$0.6_{0.1}$	$0.3_{0.1}$	<0.1	$6.0_{0.1}$	$12.0_{0.1}$	$11.1_{0.1}$	$8.5_{0.1}$
Velocity (km s^{-1})	$0.2_{0.2}$	$-1.1_{0.5}$	$-4.7_{0.3}$	$-3.4_{0.9}$		$-7.3_{0.1}$	$-2.8_{0.1}$	$-3.8_{0.1}$	$-3.8_{0.1}$
FWHM (km s^{-1})	$29.1_{0.4}$	$27.8_{1.3}$	$8.8_{0.7}$	$7.4_{2.2}$		$2.6_{0.1}$	$6.8_{0.1}$	$7.4_{0.1}$	$6.5_{0.2}$
5.88−0.39									
Amplitude (K)	$0.3_{0.1}$	$0.4_{0.1}$	$0.3_{0.1}$	$0.3_{0.1}$	<0.1	$5.3_{0.2}$	$11.5_{0.2}$	$12.7_{0.4}$	$9.9_{0.3}$
Velocity (km s^{-1})	$4.0_{0.6}$	$5.0_{1.1}$	$12.2_{0.5}$	$9.4_{0.4}$		$8.3_{0.1}$	$9.2_{0.1}$	$8.5_{0.1}$	$9.0_{0.1}$
FWHM (km s^{-1})	$54.0_{1.3}$	$59.3_{2.5}$	$14.0_{1.1}$	$4.4_{1.0}$		$1.2_{0.1}$	$4.6_{0.1}$	$3.7_{0.2}$	$3.6_{0.2}$
W3 (OH)									
Amplitude (K)	$0.4_{0.1}$	$0.2_{0.1}$	<0.1	$0.1_{0.1}$	<0.1	$0.4_{0.1}$	$7.6_{0.1}$	$5.5_{0.1}$	$5.9_{0.1}$
Velocity (km s^{-1})	$-47.7_{0.3}$	$-49.4_{1.1}$		$-47.0_{0.8}$		$-47.7_{0.2}$	$-47.1_{0.1}$	$-47.7_{0.1}$	$-47.8_{0.1}$
FWHM (km s^{-1})	$31.7_{0.6}$	$32.9_{2.6}$		$10.1_{2.0}$		$4.8_{0.5}$	$4.7_{0.1}$	$4.5_{0.1}$	$2.4_{0.1}$
351.41+0.64									
Amplitude (K)	$0.3_{0.1}$	$0.3_{0.1}$	$0.3_{0.1}$	$0.4_{0.1}$	<0.1	$2.9_{0.1}$	$13.2_{0.1}$	$9.5_{0.1}$	$8.6_{0.1}$
Velocity (km s^{-1})	$-4.5_{0.5}$	$-3.6_{0.9}$	$-9.1_{0.4}$	$-6.7_{0.4}$		$-7.6_{0.1}$	$-6.2_{0.1}$	$-7.8_{0.1}$	$-7.8_{0.1}$
FWHM (km s^{-1})	$30.1_{1.2}$	$29.2_{2.2}$	$5.8_{0.9}$	$6.9_{1.0}$		$4.6_{0.1}$	$6.2_{0.1}$	$6.1_{0.1}$	$5.0_{0.1}$
351.58−0.35									
Amplitude (K)	$0.2_{0.1}$	$0.2_{0.1}$	$0.4_{0.1}$	$0.6_{0.1}$	$0.5_{0.1}$	$0.7_{0.1}$	$3.8_{0.1}$	$2.6_{0.3}$	$1.4_{0.2}$
Velocity (km s^{-1})	$-92.7_{1.1}$	$-93.0_{1.8}$	$-98.2_{0.5}$	$-94.6_{0.4}$	$-95.8_{0.3}$	$-95.6_{0.2}$	$-97.2_{0.1}$	$-99.1_{0.1}$	$-105.6_{0.2}$
FWHM (km s^{-1})	$30.9_{2.5}$	$22.4_{4.3}$	$11.8_{1.1}$	$6.9_{1.0}$	$6.0_{0.6}$	$7.5_{0.4}$	$4.1_{0.3}$	$3.3_{0.3}$	$3.5_{0.5}$
8.68−0.37									
Amplitude (K)	$0.2_{0.1}$	$0.2_{0.1}$	<0.1	$0.3_{0.1}$	$0.4_{0.1}$	$6.4_{0.2}$	$6.1_{0.1}$	$3.9_{0.2}$	$1.8_{0.1}$
Velocity (km s^{-1})	$46.8_{0.9}$	$46.8_{2.0}$		$35.8_{0.5}$	$35.5_{0.3}$	$35.2_{0.1}$	$35.8_{0.1}$	$33.1_{0.1}$	$33.2_{0.1}$
FWHM (km s^{-1})	$24.3_{2.1}$	$23.5_{4.8}$		$5.3_{1.2}$	$3.3_{0.7}$	$3.0_{0.1}$	$7.1_{0.2}$	$2.7_{0.2}$	$2.7_{0.2}$
45.07+0.13									
Amplitude (K)	$0.2_{0.1}$	<0.2	$0.4_{0.1}$	<0.1	<0.1	<0.1	$6.1_{0.1}$	$2.7_{0.1}$	$1.7_{0.1}$
Velocity (km s^{-1})	$52.7_{1.0}$		$55.7_{0.2}$				$58.8_{0.1}$	$58.7_{0.1}$	$57.3_{0.2}$
FWHM (km s^{-1})	$22.3_{2.3}$		$2.2_{0.5}$				$6.5_{0.1}$	$6.5_{0.3}$	$12.8_{0.6}$
NGC 7538									
Amplitude (K)	$0.1_{0.1}$	<0.1	<0.2	<0.2	<0.2	$1.5_{0.1}$	$7.6_{0.1}$	$6.9_{0.1}$	$6.1_{0.1}$
Velocity (km s^{-1})	$-62.5_{1.0}$					$-57.6_{0.1}$	$-56.4_{0.1}$	$-58.3_{0.1}$	$-57.9_{0.1}$
FWHM (km s^{-1})	$15.7_{2.3}$					$2.1_{0.1}$	$6.5_{0.2}$	$4.7_{0.1}$	$4.7_{0.1}$
0.54−0.85									
Amplitude (K)	<0.3	<0.3	<0.3	$0.5_{0.1}$	<0.3	$1.6_{0.1}$	$10.8_{0.1}$	$7.3_{0.1}$	$7.6_{0.1}$
Velocity (km s^{-1})				$17.4_{0.3}$		$17.2_{0.2}$	$17.5_{0.1}$	$16.5_{0.1}$	$16.9_{0.1}$
FWHM (km s^{-1})				$5.0_{0.6}$		$6.1_{0.4}$	$6.5_{0.1}$	$5.8_{0.1}$	$4.7_{0.1}$
351.78−0.54									
Amplitude (K)	<0.3	<0.3	$1.1_{0.1}$	$1.2_{0.1}$	$0.3_{0.1}$	$15.2_{2.5}$			
Velocity (km s^{-1})			$-5.2_{0.4}$	$-2.5_{0.1}$	$-1.1_{1.0}$	$-2.4_{0.1}$	(not observed)		
FWHM (km s^{-1})			$12.4_{0.9}$	$9.2_{0.4}$	$4.1_{2.3}$	$1.4_{0.3}$			
45.47+0.13									
Amplitude (K)	<0.3	<0.3	<0.3	<0.3	<0.3	<0.3	$5.8_{0.1}$	$1.9_{0.1}$	$1.5_{0.2}$
Velocity (km s^{-1})							$61.2_{0.1}$	$62.7_{0.1}$	$62.6_{0.2}$
FWHM (km s^{-1})							$4.8_{0.1}$	$2.5_{0.3}$	$2.7_{0.4}$

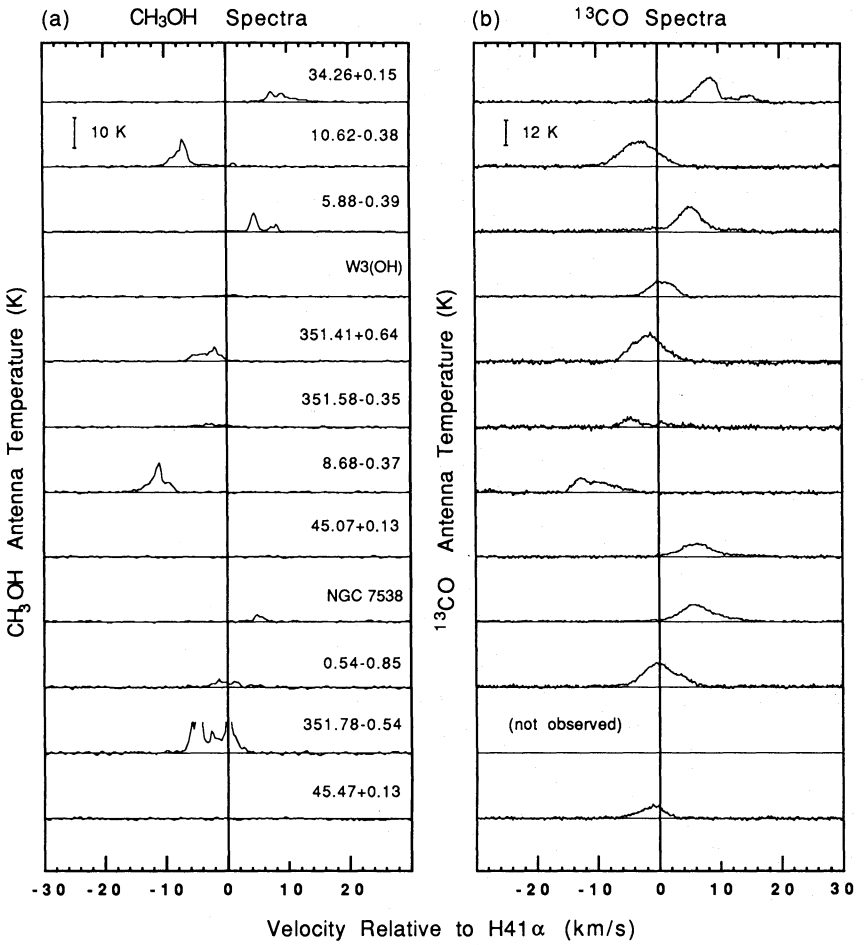

Fig. 2. a CH_3OH (44 GHz) and **b** ^{13}CO (110 GHz) spectra for the 12 sources observed. The velocities are plotted relative to H41α for the nine sources with detected H II regions. For 0.54−0.85, 351.78−0.54 and 45.47+0.13 the mean molecular line velocity has been used as the reference

maser emission. In Fig. 2 the methanol and ^{13}CO profiles are shown for all sources observed. The different character of the methanol and carbon monoxide spectra is evident, and an offset between the velocity of the molecular emission and H41α is apparent in most cases. The 15(3)–14(3) A^+ methanol transition near 89 GHz was not detected.

^{13}CO was detected toward all sources, with an average antenna temperature of ~9 K and halfwidths ranging from 4 to 7 km s^{-1}. Most of the profiles have non-Gaussian shapes; broad wings are evident in nearly all of the ^{13}CO spectra (Fig. 2b). Foreground self-absorption may be responsible for some of the structure in these profiles, particularly for 34.26+0.15. HCO^+ and HCN was also detected toward all sources, with $T_a \sim 7$ K and ~5 K respectively. The HCO^+ profiles are similar to the ^{13}CO profiles; the HCN profiles are complicated by the presence of partially blended hyperfine components. In each of the eleven sources for which offset position data was obtained, the ^{13}CO, HCO^+ and HCN intensity is strongest in the direction of the H II region or OH/H_2O maser source. For 351.41+0.64 the ^{13}CO intensity is strongest at −6 km s^{-1} while the HCO^+ and HCN lines are strongest near −9 km s^{-1}; for the other sources the molecular lines peak at approximately the same velocity. The peak intensity of these lines at each position observed is shown in Fig. 3. The brightest molecular line emission is coincident with the maser/H II complex in all cases, and appears to be at most a few beamwidths in extent.

3.3. Relative velocities

The H53α and molecular line velocities are plotted relative to the velocity of the H41α line in Fig. 4 for the nine sources containing H II regions. The relative velocities of the CH_3OH and ^{13}CO lines plotted in Fig. 2 are shown, along with the velocities of SiO, CH_3CN, HCO^+, HCN and HNCO. The mean value of the molecular line velocities is indicated by a vertical line for each source, and the offset of this value from the H41α velocity is given in a box.

The velocities of the various molecular lines in a particular source are all fairly close, and a significant offset between the mean molecular line velocity and the recombination line velocity is present for all sources except W3 (OH). The average offset is ~6 km s^{-1}, and both red- and blue-shifted offsets are equally represented. The two recombination line velocities are in generally good agreement, although for two sources (10.62−0.38 and W3 (OH)) the H53α velocity is less than the H41α velocity at a marginally significant level.

4. Discussion

4.1. Location of the molecular gas

The limited mapping done in the strong lines of ^{13}CO, HCO^+ and HCN (Fig. 3) shows that emission from these molecules peaks in the direction of the H II region/maser complex. In some cases

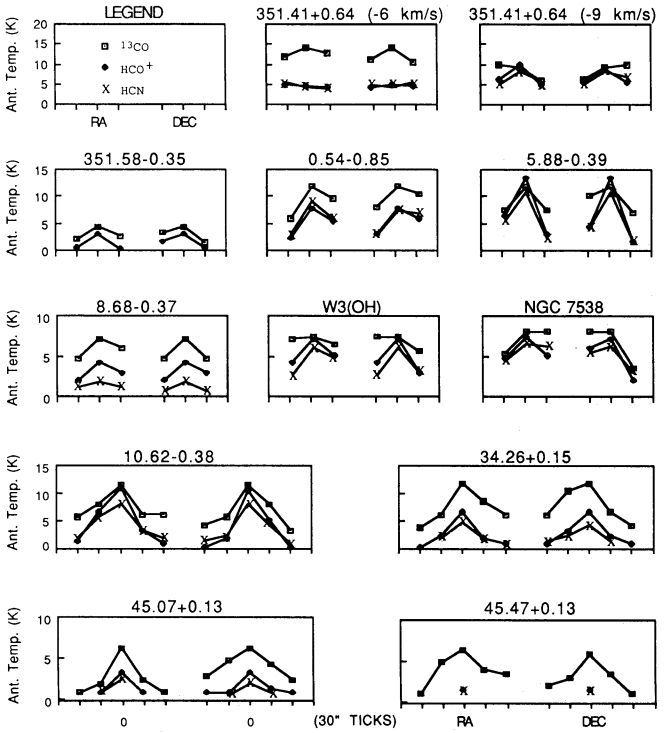

Fig. 3. The peak intensity of the ^{13}CO, HCO^+ and HCN lines is plotted versus position offset in RA and Dec for each source observed. For 351.41 +0.64 the intensity is plotted for two separate velocity components. The spatial separation between observed positions is 30″, and the central tick mark in each coordinate corresponds to the position of the maser source. No point is plotted at positions where the line was not detected

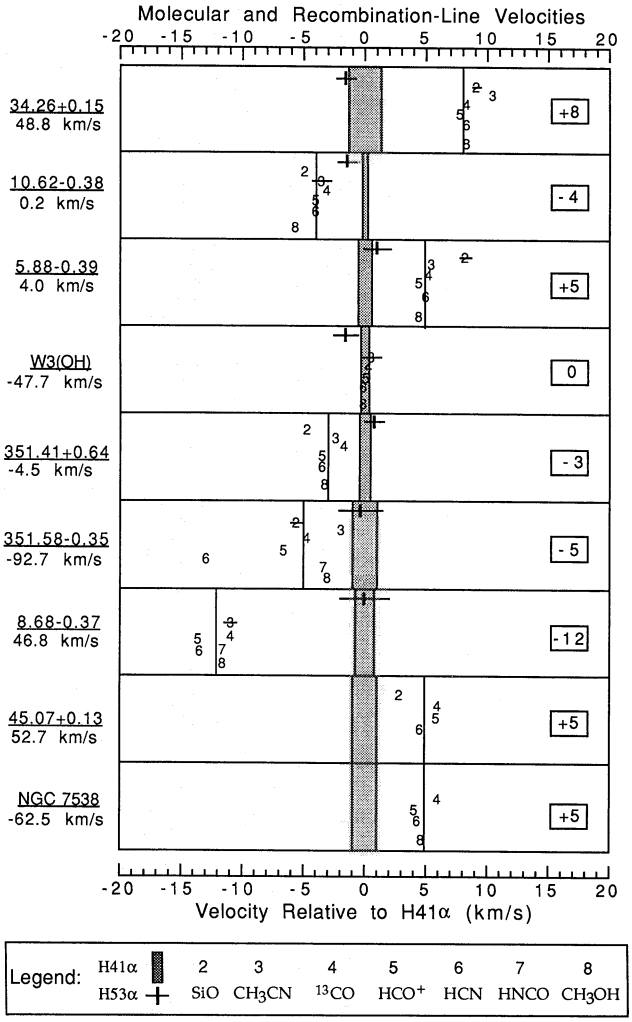

Fig. 4. Gaussian fit velocities for the detected spectral lines are plotted relative to the H41α velocity for nine sources with H II regions. The number below the source name is the velocity of the H41α recombination line. The symbols used for the spectral lines are indicated at the bottom of the figure. The width of the symbol for the recombination lines is twice the rms error in the Gaussian fit; a horizontal bar indicates the probable error for the molecular lines if the width of the associated symbol (i.e. numbers 2–8) is less than 2σ. A vertical line shows the mean velocity of the molecular lines for each source, and the box to the right gives the offset between the mean molecular line and H41α velocity

emission is still detected more than a beamwidth away indicating that the source is embedded in an extended molecular cloud. However, the strongly peaked intensity at the grid centre indicates that the strongest emission comes from a region near the source. Although no mapping data was taken in the weaker lines, they are not expected to emit strongly at the densities and temperatures typical of extended molecular clouds. It is therefore likely that emission from these lines also arises close to the newly-formed star. The fact that the observed molecular lines (with the possible exception of HNCO) appear only in emission is somewhat surprising if the H II regions are embedded in dense molecular envelopes. One possibility is that the molecular region is large compared to the H II region, and emission dominates over the Nobeyama beam. If this is the case, higher spatial resolution should show the molecular lines in absorption against the H II region.

The distribution of OH and H_2O masers has been mapped with the VLA by Forster and Caswell (1988) for all sources except W3 (OH) and NGC 7538. These two northern sources have been mapped previously by various authors (see references to Table 1). For the nine sources in this study with H II regions, the maser emission is found within ~0.2 pc of the continuum peak. For the remaining three sources without detected H II regions, the maser associations have total extents <0.2 pc. Both the OH and H_2O masers have patchy, irregular distributions, and are usually confined to only one side of the H II region. Gaume and Mutel (1987) have shown that the 18 cm OH masers tend to occur mainly along the sharpest edge of compact H II regions. At a distance of 3 kpc, the ~20″ beamwidth of the Nobeyama telescope corresponds to a linear diameter of ~0.3 pc. Our limited molecular line mapping shows that the brightest emission is coincident with the maser/H II complex, and is confined to a few beamwidths. A determination of the actual size of these molecular hotspots would require complete mapping in order to accurately define background emission levels. At the present level of accuracy, the brightest molecular line emission appears roughly coextensive with the maser complexes.

Owing to the limited number of transitions measured in the various molecular species observed, it is not possible to derive level populations accurately and establish the physical conditions pertaining in the region. The environment just beyond the ionization front of an H II region is characterized by an intense

radiation field, along with high temperature and density. In addition, shocks, stellar winds and molecular outflows from the star contribute to the complex excitation and chemistry expected in these regions. Furthermore, non-LTE conditions occur in some species, as evidenced by the presence of maser emission from OH, H_2O and CH_3OH. In the next section, the kinematics is discussed in light of the observed velocities of the ionized gas, thermally emitting molecular gas and the masers.

4.2. *Kinematics*

A significant velocity offset between the ionized gas and the molecular gas in which it is embedded is present in eight of the nine H II regions observed (Fig. 4). There is also a rather small spread in velocity among the various molecular lines detected toward each source (351.58−0.35 is an exception). This is somewhat unexpected since the upper-state energies (Table 2) and critical densities vary widely among the transitions observed. The implication of this latter result is that systematic motion in the molecular gas is moderate over the extent of the strongly emitting region. Since this gas is apparently closely associated with the H II region/maser association, we believe that the mean observed molecular line velocity provides a good estimate of the systemic velocity of the star-forming region.

If the mean molecular velocity is taken as the systemic velocity, the velocity offsets observed between the H II region and the molecular gas points to ordered motion in the ionized gas. A likely cause of such motion is a density gradient. This could occur if the H II region is located near the edge of a molecular cloud, as in the blister model proposed for Orion by Zuckerman (1973). As the H II region expands due to thermal pressure, the expansion proceeds most rapidly in the direction of decreasing density. This causes a flow of ionized gas away from the denser parts of the surrounding molecular cloud. While the flow will, of course, impart some momentum to the molecular gas, we expect the gas to have too much inertia for this to cause a significant velocity shift in the molecular lines. The magnitude of the offsets measured in our sample (up to 12 km s^{-1}) is consistent with expansion of a 10^4 K H II region at the sound speed of $\sim$15 km s^{-1}.

A variety of molecules having a range of critical densities have been included in this study. The uniformity in velocity among the various molecular species is therefore rather surprising. Although no systematic velocity offset between low and high-excitation molecules is found, the ^{13}CO and HCO^+ profiles have wings typically $\sim$10 km s^{-1} in extent. The wings are not correlated with the magnitude or direction of the recombination line offsets observed, however. While an origin related to the ionized flow can be hypothesized, the nature of the relationship is not clear.

A location near the edge of a molecular cloud is one way of providing a density gradient, but any inhomogeneous gas distribution could produce a flow. Even deeply embedded H II regions will develop systematic motion if density structure is present. In order to maintain an essentially Gaussian recombination line profile, however, most of the ionized gas must be involved in the flow. The scale-size of the inhomogeneity must therefore be comparable to the size of the H II region. The high percentage of sources in our sample which exhibit a significant velocity offset suggests that most H II regions occur in a non-uniform environment.

Wood and Churchwell (1989) suggest that the morphology of arc-shaped H II regions is caused by density enhancement in front of a young star which is moving relative to the surrounding molecular cloud. A density gradient set up by the bow shock will produce an ionized flow in the direction opposite to the motion of the star. If the star formed in the inertial frame of the molecular cloud, however, the source of the translational motion is not clear. Other ways of producing density gradients for deeply embedded objects include formation of discs or torus', and density structures caused by shocks or outflows from other objects nearby.

Expansion of the H II region is required in order to set up an ionized flow in the direction of a density gradient. For an expanding H II region, optical depth effects are important in determining the recombination line velocity observed (e.g. Berulis and Ershov, 1983; Welch and Marr, 1987). Lower-frequency recombination line velocities have been reported for some of the H II regions in this study (see references for Table 1), and there is a clear tendency for the velocity to increase with frequency. The slightly higher velocity measured for H41α compared to H53α in W3 (OH) and 10.62−0.38 (Fig. 4) may be due to this effect. For a 10^4 K H II region of diameter 0.1 pc and electron density of 10^5 cm^{-3}, the optical depth is $\sim$0.2 at 43 GHz, so opacity effects could affect the H53α velocity. However, directed flow rather than spherical expansion appears to be the dominant motion in these H II regions.

4.3. *Masers*

Garay et al. (1985) measured systematically red-shifted offsets between the velocity of OH maser emission and the recombination line velocity at 15 and 22 GHz toward nine H II regions, four of which are common to our sample. The consistent redshift, along with the assumption that the OH masers are seen only on the near side of the H II region, led them to conclude that OH masers arise in material which is still accreting. The OH masers associated with the H II regions in our sample have median velocities within a few km s^{-1} of the mean molecular line velocity. The velocity offsets measured between the H41α and the molecular lines therefore apply also to the OH masers. We find no preference for the OH masers to occur red-shifted with respect to the recombination line velocity, although an offset to one side or the other is usually present. Since lower frequency recombination lines are systematically bluer, optical depth effects could account for the results of Garay et al.

H_2O masers frequently exhibit weak features at velocities as great as 50 km s^{-1} from stronger features near the systemic velocity. H_2O spectra for the seven southern H II regions in our sample are shown in Fig. 5, with the velocities plotted relative to the H41α velocity. The mean molecular line velocity is indicated for each source, and the full range of detected H_2O features is shown by a horizontal bar. Owing to the variability of H_2O masers, the maximum and minimum velocity features were determined using a database which includes spectra taken over a two year period (Marshall, 1987). The H_2O masers exhibit spectral features which are displaced asymmetrically around the molecular line velocities. In five cases (34.26+0.15 and 351.58−0.35 are exceptions) the H_2O maser velocities extend furthest in the same direction as the velocity offset between the molecular lines and the H41α recombination line. This indicates that high-velocity H_2O masers tend to move in the direction opposite to the ionized flow, i.e. towards higher density. This is consistent with the model of Tarter and Welch (1986) in which ejecta from star-forming regions are collisionally excited by

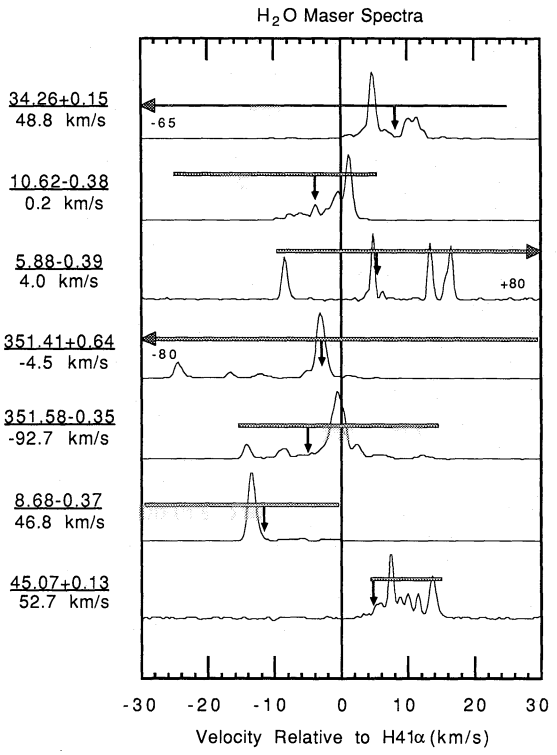

Fig. 5. H_2O maser spectra plotted relative to the H41α velocity. The total velocity extent of the maser emission is indicated by a horizontal bar, and the minimum or maximum velocities of detected H_2O features are noted in the three cases where they extend beyond the limits of the velocity scale shown. A vertical arrow marks the position of the mean molecular line velocity for each source. The H_2O masers exhibit spectral features which are displaced asymmetrically around the molecular line velocities. In five cases (34.26 + 0.15 and 351.58 − 0.35 are exceptions) the H_2O maser velocities extend furthest in the same direction as the velocity offset between the molecular lines and the H41α recombination line. The number below the source name is the H41α velocity

collisions with ambient molecular material. Even if matter is ejected isotropically, collisional excitation in this direction will be enhanced by the higher ambient density.

5. Summary

Two hydrogen recombination lines and seven molecular lines were observed toward nine compact H II regions with OH and H_2O maser emission and three OH/H_2O maser associations without detected H II regions. RA and Dec offset spectra show that the molecular lines peak at the position of the H II region or maser complex, and that the emission is fairly compact. The 7(0)–6(1) A^+ methanol transition near 44 GHz is probably masing in at least six of these sources.

Velocity offsets of typically 6 km s^{-1} are found between the ionized gas and the molecular gas in these sources. In four cases the ionized gas is red-shifted with respect to the molecules, in four cases it is blue-shifted, and in W3 (OH) the shift is zero. High-velocity H_2O masers tend to occur at velocities shifted with respect to the molecular lines in the opposite sense from the ionized gas, and with larger velocity offsets. We suggest that the molecular lines arise in dense, relatively stationary material adjacent to the H II region. The H41α velocity offset is caused by bulk motion of the ionized gas as the H II region expands in the direction of decreasing density. High-velocity H_2O masers occur mainly in the opposite direction, towards higher density, and probably represent ejecta from the star colliding with the ambient material.

Acknowledgements. We are indebted to the late Hiroko Suzuki for her help with the data reduction, and thank the staff of the Nobeyama 45 m telescope for helping with the observations.

References

Benson, J.M., Johnston, K.J.: 1984, *Astrophys. J.* **277**, 181
Berulis, I.I., Ershov, A.A.: 1983, *Sov. Astron. Lett.* **9**, 341
Campbell, B.: 1984, *Astrophys. J.* **282**, L27
Dreher, J., Welch, W.J.: 1981, *Astrophys. J.* **245**, 857
Forster, J.R., Caswell, J.L.: 1988, *Astron. Astrophys.* **213**, 339
Forster, J.R., Welch, W.J., Wright, M.C.H., Baudry, A.: 1978, *Astrophys. J.* **221**, 137
Garay, G., Reid, M.J., Moran, J.M.: 1985, *Astrophys. J.* **289**, 681
Gaume, R.A., Mutel, R.L.: 1987, *Astrophys. J. Suppl.* **65**, 193
Ho, P.T.P., Haschick, A.D.: 1981, *Astrophys. J.* **248**, 622
Ho, P.T.P., Haschick, A.D., Vogel, S.N., Wright, M.C.H.: 1983, *Astrophys. J.* **265**, 295
Lovas, F.J.: 1986, *J. Phys. Chem. Ref. Data* **15**, 251
Lilley, A.E., Palmer, P.: 1968, *Astrophys. J. Suppl.* **16**, 143
Marshall, G.L.: 1987, *H_2O maser data system*, Internal report, CSIRO; Div. Radiophysics
Norris, R.P., Booth, R.S.: 1981, *Monthly Notices Roy. Astron. Soc.* **195**, 213
Reid, M.J., Haschick, A.D., Burke, B.F., Moran, J.M., Johnston, K.J., Swenson, G.W.: 1980, *Astrophys. J.* **239**, 89
Rodriguez, L.F., Canto, J., Moran, J.M.: 1982, *Astrophys. J.* **255**, 103
Rots, A.H., Dickel, H.R., Forster, J.R., Goss, W.M.: 1981, *Astrophys. J. Lett.* **245**, L15
Turner, B.E., Matthews, H.E.: 1984, *Astrophys. J.* **277**, 164
Welch, W.J., Marr, J.: 1987, *Astrophys. J. Lett.* **317**, L21
Wilson, T.L., Mauersberger, R., Brand, J., Gardner, F.F.: 1987, *Astron. Astrophys. Lett.* **186**, L5
Tarter, J.C., Welch, W.J.: 1986, *Astrophys. J.* **305**, 467
Wood, D.O.S., Churchwell, E.: 1989, *Astrophys. J. Suppl.* **69**, 831
Zuckerman, B.: 1973, *Astrophys. J.* **183**, 863